

# Tuning the band topology and topological Hall effect in skyrmion crystals via the spin-orbit coupling

Arijit Mandal and B. R. K. Nanda\*

*Condensed Matter Theory and Computational Lab,  
Department of Physics, IIT Madras, Chennai-600036, India and  
Center for Atomistic Modelling and Materials Design, IIT Madras, Chennai-600036, India*

S. Satpathy†

*Condensed Matter Theory and Computational Lab,  
Department of Physics, IIT Madras, Chennai-600036, India  
Center for Atomistic Modelling and Materials Design, IIT Madras, Chennai-600036, India and  
Department of Physics & Astronomy, University of Missouri, Columbia, MO 65211, USA*

The topological Hall effect (THE) is the result of spin-asymmetric deflection of charge carriers flowing through a non-collinear spin system. Effective manipulation of the topological Hall conductivity (THC) in skyrmions is currently a vigorous area of research with an eye towards potential spintronics application. Here, we show that the band topology and the THC in a skyrmion crystal can be tuned by changing the strength of the Rashba spin-orbit coupling (SOC), which can be accomplished via a perpendicular electric field. This results in the change of the subband Chern numbers and a transition between ordinary insulator and Chern insulator as the Rashba SOC is varied. For partially filled subbands, the Rashba SOC can tune the THC and reverse its sign, so that the direction of the Hall current is flipped. The critical Rashba strength for this depends on the skyrmion type and the carrier density. We extend our analysis to the cases of Dresselhaus and Weyl SOC as well, and show that they can be directly mapped to the Rashba SOC case and therefore lead to similar results. Our work suggests new avenues for the control of charge transport in skyrmion crystals.

## I. INTRODUCTION

Skyrmions are topologically protected structures that have garnered significant attention in recent years for the fundamental science as well as for potential application in spintronics devices[1–9]. Originally proposed by Skyrme[1] as a model for baryons in particle physics in the 1960s, they have found widespread application in condensed matter physics including Bose-Einstein condensates[10, 11], liquid crystals[12], quantum Hall magnets[13, 14], and helimagnets[2, 15]. The magnetic skyrmions that form in the solid are nanometer-size twirling spin structures, which are metastable due to the topological protection with a fixed quantized winding number.

Since the prediction of the stable skyrmion state in magnetic solids[2], skyrmions have been observed in a plethora of materials [7] such as the ferromagnetic semiconductors with B20 structure such as MnSi and FeGe[16, 17], transition metal oxides [18, 19], Heusler alloys [20], Janus materials [21], moiré heterostructures [22], intermetallic compounds [23], and magnetic multilayers [24]. Skyrmion crystals, the ordered arrays of skyrmions, have been suggested theoretically[25] in magnets as well as in two-dimensional electron gas[26]. Several theoretical studies have also examined the energetics of the formation of stable skyrmion crystals via

Dzyaloshinskii–Moriya interaction, magnetic frustration, anisotropy, etc.[25, 27–35]

Experimentally, skyrmion crystals have been observed in several systems using neutron scattering and Lorentz transmission electron microscopy. A hexagonal skyrmion lattice was first observed in MnSi [16] and later in other intermetallics such as FeCoSi, FeGe, and Co<sub>8</sub>Zn<sub>10</sub>Mn<sub>2</sub> [36–39]. Other types of lattices have been found as well, viz., the triangular lattice in Gd<sub>2</sub>PdSi<sub>3</sub>, Gd<sub>3</sub>Ru<sub>4</sub>Al<sub>12</sub>, and the CoZnMn alloy system[40–42], as well as the square lattice in GdRu<sub>2</sub>Si<sub>2</sub>, EuAl<sub>4</sub>, and in monolayer Fe/Ir(111) [43–45].

The transport of electrons in the presence of skyrmions has emerged as an important area of research. Included in this are the topological Hall effect (THE) and the spin Hall effect (SHE) as well as the skyrmion Hall effect, which concerns the transport of the skyrmions themselves[46]. THE arises from the transverse motion of electrons due to the emergent magnetic field of the non-collinear spin texture, an effect akin to the anomalous Hall effect (AHE) in the collinear spin system.

There has been mounting interest in the electrical field control of the Hall effects because it would enable spin manipulation without an external magnetic field or a large current injection. However, there has been limited success in this direction using conventional field-effect structures involving magnetic materials adjacent to gate dielectrics. More recently, it has been suggested that this may be achieved through the spin-orbit coupling (SOC) effect, which may be modified by an applied electric field. In a recent experiment, it was found that

\* nandab@iitm.ac.in

† satpathys@missouri.edu

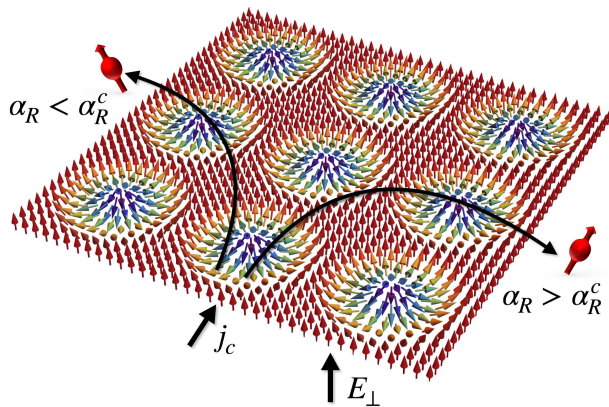


FIG. 1. Topological Hall effect in the skyrmion crystal. The magnitude of the Hall current can be changed and its sign can be reversed by tuning the Rashba SOC through a critical value  $\alpha_R^c$ . The Rashba strength  $\alpha_R$  can be modified via a perpendicular electric field  $E_\perp$  or by growing an overlayer. Similar effects can be obtained with the Dresselhaus and Weyl SOC also as discussed in the text.

both the AHE and the THE (arising from the interfacial skyrmions) can be tuned by an applied electric field in the oxide heterostructure via the SOC effect of an inserted layer[47, 48].

In this work, we study the THE in the skyrmion crystal in the presence of three types of SOC, viz., the Rashba, Dresselhaus, or the Weyl type. The Rashba case is studied in some detail, while we show that the other two cases can be mapped to the Rashba case for the skyrmion types we have considered here. Quite remarkably, we find that not only can the magnitude of the THC be significantly changed by varying the strength of the Rashba SOC via an applied electric field, but also that the sign of the Hall conductivity can be reversed by varying the Rashba SOC around a critical value. The band topology in the skyrmion crystal can also be changed by varying the strength of the SOC term, resulting in a change in the subband Chern numbers, which can lead to a flipping of the direction of the topological edge current.

## II. MODEL HAMILTONIAN AND THE ELECTRON BAND STRUCTURE

We consider the model Hamiltonian for a square lattice for an electron moving through the skyrmion crystal in the presence of the Rashba SOC

$$\begin{aligned} \mathcal{H} = & -t \sum_{\langle ij \rangle} (c_i^\dagger c_j + c_j^\dagger c_i) - J \sum_i \mathbf{S}_i \cdot c_i^\dagger \boldsymbol{\sigma} c_i \\ & - i\alpha_R \sum_{\langle ij \rangle} c_i^\dagger (\boldsymbol{\sigma} \times \mathbf{r}_{ij})_z c_j + H.c.. \end{aligned} \quad (1)$$

The first term is the nearest neighbor hopping term, where we have suppressed the spin index, with  $c_i^\dagger \equiv$

$(c_{i\uparrow}^\dagger, c_{i\downarrow}^\dagger)$  and  $c_i \equiv (c_{i\uparrow}, c_{i\downarrow})^T$ ,  $i$  is the site index on the lattice,  $\sigma$  is the spin index,  $c_{i\sigma}^\dagger/c_{i\sigma}$  are the corresponding electron creation/annihilation operators,  $\langle ij \rangle$  indicates distinct pairs of nearest neighbors, and H. c. indicates Hermitian conjugate of the last term only. The second term is the exchange interaction between the site-fixed spins  $\mathbf{S}_i$ , commonly taken as classical spins, with the skyrmion texture and  $\boldsymbol{\sigma}$  is the Pauli matrix describing the electron spin. The third term is the lattice version of the Rashba SOC[49, 50], which breaks the  $z \rightarrow -z$  symmetry. In this term,  $\alpha_R$  is the Rashba interaction strength and  $\mathbf{r}_{ij} = \mathbf{r}_j - \mathbf{r}_i$  is the vector distance between the nearest-neighbor sites. It is easily shown that (Supplementary Materials) for the free-electron case (small  $k$  limit of the lattice case), it yields the well-known form of the Rashba Hamiltonian  $\mathcal{H}_R^k = \alpha'_R (\boldsymbol{\sigma} \times \mathbf{k}) \cdot \hat{z}$ , with a scaled coefficient  $\alpha'_R = 2a^2\alpha_R$ , with  $a$  being the lattice constant. The Rashba SOC can arise due to the symmetry breaking due to an overlayer or by applying an external electric field. For the free electrons in the presence of an electric field, the strength of the Rashba term is given by  $\alpha'_R = \hbar^2 E_z / 2m_e^2 c^2$ . However, for the solids, it is enormously enhanced owing to the fact that the relativistic effects originate largely from the nuclear region[51].

The exchange interaction is often taken as  $J \rightarrow \infty$ , which is reasonable considering that for typical solids  $J \sim 2 - 3$  eV, while the typical hopping is a fraction of an eV. Also, the essential physics discussed here is not changed by taking this limit. However, there are no additional complications if a general  $J$  is used. In infinite  $J$  limit, the problem reduces to that of the spinless fermions, since the electron state with spin anti-aligned with the lattice spin is forbidden. The spinless fermion operators are described by

$$d_i^\dagger = \cos(\theta_i/2) c_{i\uparrow}^\dagger + e^{i\phi_i} \sin(\theta_i/2) c_{i\downarrow}^\dagger, \quad (2)$$

where  $(\theta_i, \phi_i)$  is the orientation of the lattice spins in spherical coordinates. The Hamiltonian assumes the form

$$\begin{aligned} \mathcal{H}_R = & -t \sum_{\langle ij \rangle} \cos \frac{\theta_{ij}}{2} e^{ia_{ij}} d_i^\dagger d_j \\ & - i\alpha_R \sum_{\langle ij \rangle} [e^{i\phi_j} (r_{ij}^y + ir_{ij}^x) \cos \frac{\theta_i}{2} \sin \frac{\theta_j}{2} \\ & + e^{-i\phi_i} (r_{ij}^y - ir_{ij}^x) \cos \frac{\theta_j}{2} \sin \frac{\theta_i}{2}] d_i^\dagger d_j + H.c., \end{aligned} \quad (3)$$

where the electronic hopping is reduced by the factor  $\cos(\theta_{ij}/2)$  and the Peierls phase factor  $e^{ia_{ij}}$  indicates the presence of the emergent magnetic field, which turns the spin of the electron as it moves from site to site. In Eq. (3),  $\theta_{ij} = \cos^{-1}(\sin \theta_i \sin \theta_j \cos(\phi_i - \phi_j) + \cos \theta_i \cos \theta_j)$  and  $a_{ij} = -\tan^{-1}[\sin(\phi_i - \phi_j)/(\cot(\theta_i/2) \cot(\theta_j/2) + \cos(\phi_i - \phi_j))]$ , and the subscript in  $\mathcal{H}_R$  has been added to distinguish it from the Dresselhaus and Weyl Hamiltonians,  $\mathcal{H}_D$  and  $\mathcal{H}_W$ , discussed later. In an earlier work[52],

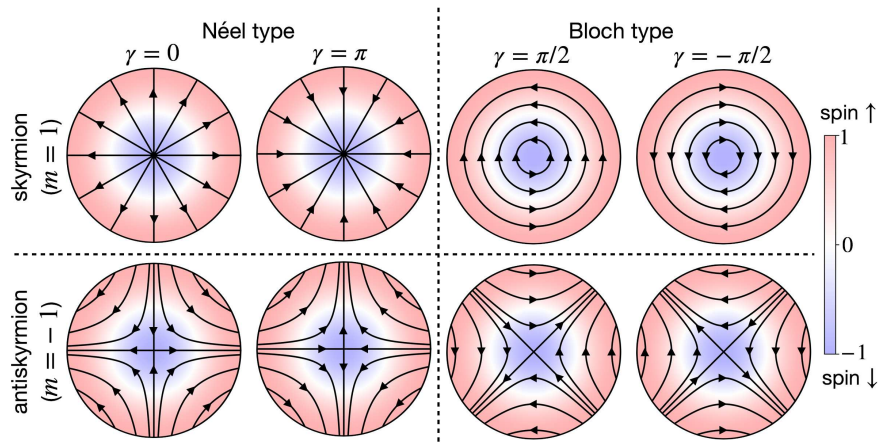


FIG. 2. Illustration of the skyrmion spin texture using field lines. The tangent indicates the planar component of the local skyrmion spin, while the color indicates the component normal to the plane. The spin at the origin is pointed down, changing gradually to the spin up orientation at the skyrmion boundary, as indicated by the color coding.

we have found that the presence of the Rashba or the Dresselhaus SOC affects the electron motion in such a way that the electron can form a self-trapped bound state at the skyrmions core, if the conditions are right.

We take the spin texture of the isolated skyrmion in the form

$$\theta(r) = \begin{cases} \pi(1 - r/\lambda) & \text{for } r \leq \lambda \\ 0 & \text{for } r > \lambda, \end{cases} \quad (4)$$

$$\phi(\alpha) = m\alpha + \gamma,$$

where  $(\theta, \phi)$  are the polar and azimuthal angles in the spherical polar coordinates and  $(r, \alpha)$  is the 2D position of the lattice spin in polar coordinates with the origin coinciding with the skyrmion centre. Here,  $\lambda$  is the skyrmion radius,  $m$  is the winding number or the vorticity, and  $\gamma$  is the helicity of the skyrmion. For a single-turned skyrmion and antiskyrmion,  $m$  takes the value of +1 and -1, respectively. Depending on the helicity, skyrmions can be classified as Néel ( $\gamma = 0$  or  $\pi$ ) and Bloch types ( $\gamma = \pm\pi/2$ ) as illustrated in Figure 2.

We consider a square lattice of localized spins with a magnetic unit cell of  $N \times N$  sites hosting a skyrmion with the spin texture Eq. 4. Thus the skyrmions form a square lattice with lattice constant  $Na$ , where  $a = 1$  is the distance between the neighboring spins. We took  $N = 4$  with the skyrmion radius  $\lambda = 2a$ , so that there are  $N^2 = 16$  sites in the magnetic unit cell of the skyrmion crystal. Other skyrmion/antiskyrmion crystals are defined in a similar way.

The SOC modifies the emergent magnetic field of the skyrmion, which we discuss below. In addition, it modifies the magnitude of the effective hopping (see Supplementary Materials for details). Both these effects modify the electronic band structure as well as the topological properties.

*Emergent magnetic field.* In the lattice models with a magnetic field, hopping integrals between lattice sites ac-

quire a complex phase factor  $t \times \exp\left[\frac{-ie}{\hbar} \int_a^b \mathbf{A} \cdot d\mathbf{r}\right]$  via the Peierls substitution, where  $t$  is the hopping without the magnetic field,  $\mathbf{A}$  is the vector potential,  $-e < 0$  is the charge of the electron, and the integral is taken over the path joining the two sites. To compute the magnetic field, we take an infinitesimal square loop around the point  $\mathbf{r}$  and compute the flux through it using the Peierls phase factors accumulated by the electron as it travels around the square loop, following the Hamiltonian Eq. (3). Note that the magnetic field is independent of the lattice type of the skyrmion crystal (square lattice in this paper). After straightforward but tedious algebra, we find that the magnetic field, which is normal to the skyrmion plane, is given by

$$B_{SK}^R(r) = \frac{\Phi_0}{2\pi} \times \left[ \frac{\pi}{2\lambda r} \sin \frac{\pi r}{\lambda} - \frac{\alpha_R}{t} \left( \frac{\pi}{\lambda} \cos \frac{\pi r}{\lambda} + \frac{1}{r} \sin \frac{\pi r}{\lambda} \right) \cos \gamma \right] \quad (5)$$

for  $r < \lambda$ , and zero for  $r > \lambda$ , and  $\Phi_0 = h/e$  is the flux quantum. The first term is due to the skyrmion alone and the second term is the modification due to the Rashba SOC. The superscript in  $B_{SK}^R$  refers to the Rashba SOC case. For the antiskyrmion, the expression is

$$B_{AS}^R(r, \alpha) = \frac{\Phi_0}{2\pi} \times \left[ -\frac{\pi}{2\lambda r} \sin \frac{\pi r}{\lambda} - \frac{\alpha_R}{t} \left( \frac{\pi}{\lambda} \cos \frac{\pi r}{\lambda} - \frac{1}{r} \sin \frac{\pi r}{\lambda} \right) \cos(2\alpha - \gamma) \right] \quad (6)$$

where the magnetic field is no longer circularly symmetric. It can be shown by direct integration that the total flux passing through a single skyrmion/antiskyrmion is  $\pm\Phi_0$ , irrespective of the strength of the Rashba term.

*Electron band structure.* Electron states in a lattice with a uniform magnetic field has been long studied since the seminal work of Hofstadter[53] that produced the celebrated ‘‘Hofstadter butterfly’’ graph for the al-

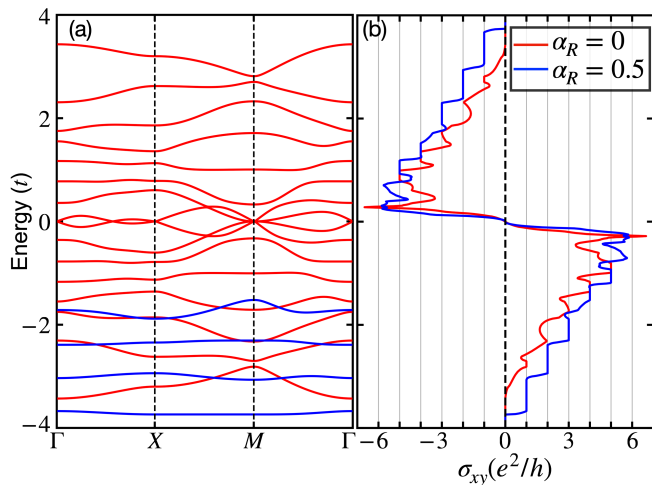


FIG. 3. Band structure and THC in the skyrmion crystal with the Néel skyrmion. (a) Band structure without (red lines) and with (blue lines) Rashba SOC. For the latter case, only the lowest four bands are shown. (b) THC as a function of the Fermi energy  $\epsilon_F$ , indicating prominent Hall plateaus for  $\alpha_R = 0.5t/a$ , chosen so as to produce a maximally uniform magnetic field (see Fig. 4).

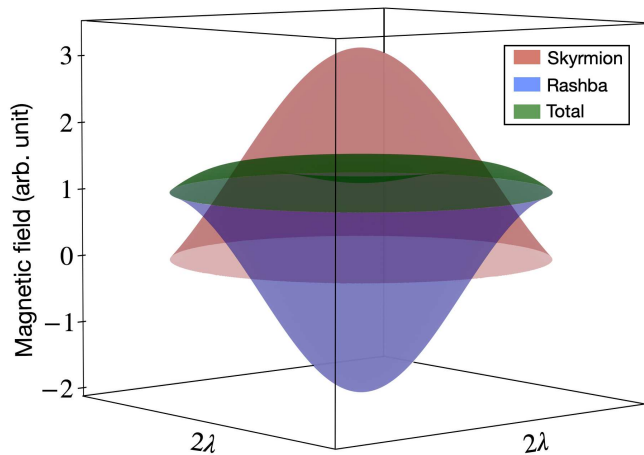


FIG. 4. Emergent magnetic field, in arbitrary units, from Eq. (5) due to the Néel skyrmion (red) and the Rashba SOC term with  $\alpha_R = 0.541/\lambda$  (blue), which add up to a near-uniform total magnetic field (green).

lowed energy regions. In our problem, we have a non-uniform magnetic field and also we are interested in the band structure and its topological properties. This has been examined in the literature for several lattices starting with the pioneering work of Hamamoto et al.[54], where the connection between the subbands and the Landau levels for the free electrons in a uniform magnetic field was made. The subband energies for the lattice case can be estimated[55] by using the Bohr-Sommerfeld semiclassical quantization rules, which was originally applied by Onsager[56] to discuss the de Haas-van Alphen oscillations in solids. Our work extends these

ideas to systems where the SOC is present. We consider three types of SOC terms, viz., the Rashba, Dresselhaus, and Weyl SOC, which may be engineered to be present under appropriate circumstances. For example, it has been demonstrated that the relative strengths of the Rashba and Dresselhaus SOC terms can be tuned experimentally in semiconductor quantum wells via interface engineering[57] and electric field[58].

We first consider the square lattice of single-turned Néel type skyrmion with helicity  $\gamma = 0$ . The band structures with and without a Rashba SOC are shown in Figure 3. The non-uniform magnetic field produces a larger subband dispersion (red curves in Figure 3 (a)) as compared to the case of the uniform magnetic field. The Rashba term modifies the emergent magnetic field, as discussed already, which in turn modifies the band structure. An interesting situation arises, where by adjusting the strength of the Rashba term, one can make the emergent magnetic field nearly uniform. In that case, the band structure will resemble the Landau level bands for the uniform magnetic field.

To obtain this optimal value  $\alpha_R^0$  that produces the maximally uniform magnetic field, we have minimized the smoothness integral  $\int_0^\lambda 2\pi r (dB_{SK}(r)/dr)^2 dr$  over the skyrmion radius using the total magnetic field Eq. (5). The result is:

$$\alpha_R^0 = (\pi t/\lambda)(2c - 1)(\pi^2 - 2 + 6c)^{-1} \approx 0.54 t/\lambda, \quad (7)$$

where  $c = c_1 - c_2 + \ln(2\pi)$ ,  $c_1 \approx 0.577$  is the Euler-Mascheroni constant, and  $c_2 = -\int_{2\pi}^\infty dx \cos x/x \approx -0.022$  is the cosine integral. From an inspection of Eq. (5), it is obvious that the magnetic field can never be uniform for all  $r$ , but for the optimal Rashba strength  $\alpha_R^0$ , we find that the rms deviation of  $B(r)$  from the mean is as small as  $\approx 8\%$ . Fig. 4 shows the magnetic field for the optimal value  $\alpha_R^0$ .

The optimal value expression for  $\alpha_R^0$ , Eq. (7), was obtained in the continuum limit. However, in the skyrmion crystal, because only a small number of lattice points sample the skyrmion magnetic field (for our square lattice there are only  $4 \times 4$  lattice points in the magnetic unit cell containing a single skyrmion), the optimal  $\alpha_R^0$  is different from the predicted value, which is more accurate for very large magnetic cells. Test calculations with  $100 \times 100$  unit cell yielded the  $\alpha_R^0$  value as predicted by Eq. (7). In the present case of the  $4 \times 4$  magnetic unit cell,  $\alpha_R^0$  is found to be about twice of Eq. (7).

The band structure for the  $4 \times 4$  lattice with the Rashba strength  $\alpha_R^0$  is shown in Figure 3 (a) (in blue), which is very similar to the bands with a uniform magnetic field (see Supplementary Materials). As discussed in the next Section, we show that the topology of the bands become modified in the presence of the Rashba SOC term, which in turn leads to the tuning and sign reversal of the THC.

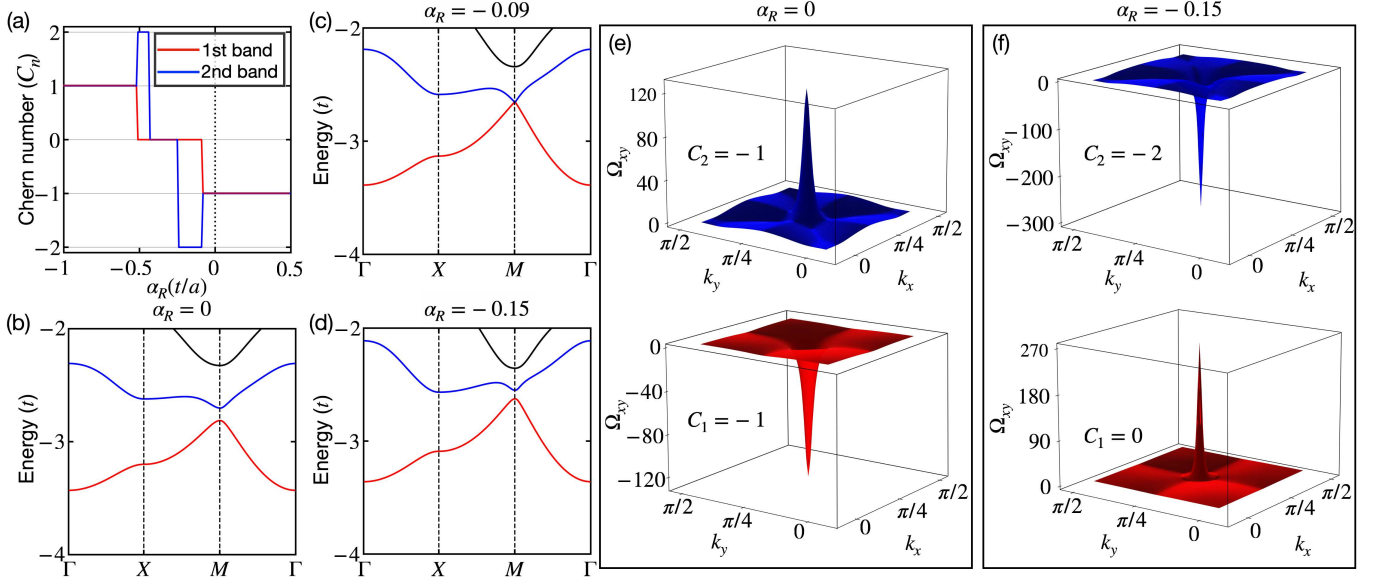


FIG. 5. Tuning the band topology with the Rashba SOC for the Néel type skyrmion crystal. (a) The Chern number of the lowest two subbands as a function of  $\alpha_R$ . (b, c, d) Evolution of the band structure with  $\alpha_R$  changing through the crossover point  $\alpha_R \approx -0.09$ . The lowest two subbands touch and separate, and their Chern numbers change. (e, f) Berry curvatures for the lowest two subbands for  $\alpha_R$  just above and below the crossover point, corresponding to the band structure of (b) and (d) respectively.

### III. TOPOLOGICAL HALL EFFECT WITH RASHBA SOC

The THC can be computed as a sum of the Berry curvature in the momentum space following the standard expression [59]

$$\sigma_{xy} = -\frac{e^2}{\hbar} \frac{1}{N_k A} \sum_{n\mathbf{k}} f(\varepsilon_{n\mathbf{k}}) \Omega_n^z(\mathbf{k}), \quad (8)$$

where  $N_k$  is the number of  $\mathbf{k}$ -points in the BZ,  $A$  is the area of the unit cell,  $\varepsilon_{n\mathbf{k}}$  is the band energy, and  $f(\varepsilon_{n\mathbf{k}})$  is Fermi-Dirac distribution function. The Berry curvature  $\vec{\Omega}(\vec{k})$  enters into the semiclassical equation of motion for the Bloch electron and affects the motion of the wave packet if it is non-zero. The velocity of the Bloch electron wave packet is given by the expression[59]

$$\dot{\vec{r}}_{n\vec{k}} = \hbar^{-1} [\vec{\nabla}_{\vec{k}} \varepsilon_{n\vec{k}} + e\vec{E} \times \vec{\Omega}_n(\vec{k})], \quad (9)$$

where the second term on the right hand side is the “anomalous velocity”  $\vec{V}_{n\vec{k}} = (e/\hbar)\vec{E} \times \vec{\Omega}_n(\vec{k})$ . The Berry curvature  $\Omega_n^z(\mathbf{k})$  of the  $n$ -th band may be evaluated from the Kubo formula

$$\Omega_n^z(\mathbf{k}) = -2\hbar^2 \text{Im} \sum_{m \neq n} \frac{\langle \psi_{n\mathbf{k}} | v_\alpha | \psi_{m\mathbf{k}} \rangle \langle \psi_{m\mathbf{k}} | v_\beta | \psi_{n\mathbf{k}} \rangle}{(\varepsilon_{m\mathbf{k}} - \varepsilon_{n\mathbf{k}})^2}, \quad (10)$$

where the velocity operator  $v_\alpha = (\hbar^{-1}) \partial \mathcal{H} / \partial k_\alpha$ ,  $(\alpha, \beta, \gamma)$  are cyclic permutations of  $(x, y, z)$ , and  $\varepsilon_{m\mathbf{k}}$  and  $\psi_{m\mathbf{k}}$  are the band energies and the wave functions. In the rest of

the paper, we drop the subscripts in the THC  $\sigma_{xy}$  and simply call it  $\sigma$ .

The Chern number, defined as the sum of the Berry curvature over the Brillouin zone

$$C_n = \frac{1}{2\pi} \int_{BZ} d\mathbf{k} \Omega_n^z(\mathbf{k}), \quad (11)$$

is an important integer quantity that characterizes the topology of the band,  $n$  being the band index. For a completely filled band, its contribution to the Hall conductivity is simply  $\sigma = -(e^2/\hbar) C_n$ , and  $C_n \neq 0$  indicates a non-trivial topological band.

The THC in the skyrmion crystal without the Rashba SOC has been studied by earlier authors for several lattices. The results for the square lattice are shown in the Figure 3 both without and with the Rashba SOC term. When the Rashba SOC is absent, the Chern number for each of the subband is  $C_n$  of  $-1$  as in the case of LLs arising from the uniform magnetic field [54, 55], except for the cluster of subbands around the van Hove singularity at  $E = 0$ , which have the collective Chern number of  $N - m$  as a group, where  $N$  is the total number of subbands (16 here) and  $m$  is the number of subbands in the cluster. If the Fermi level lies within a band gap, the THC is simply the negative of the sum of the Chern numbers of the lower bands in units of  $e^2/h$ . Due to the overlapping bands, these plateaus are not always visible.

With the introduction of the Rashba SOC, the band dispersion is modified, and at an optimal value  $\alpha_R^0$ , the subbands become nearly dispersionless as discussed earlier. At this point, the THC quantization plateaus promi-

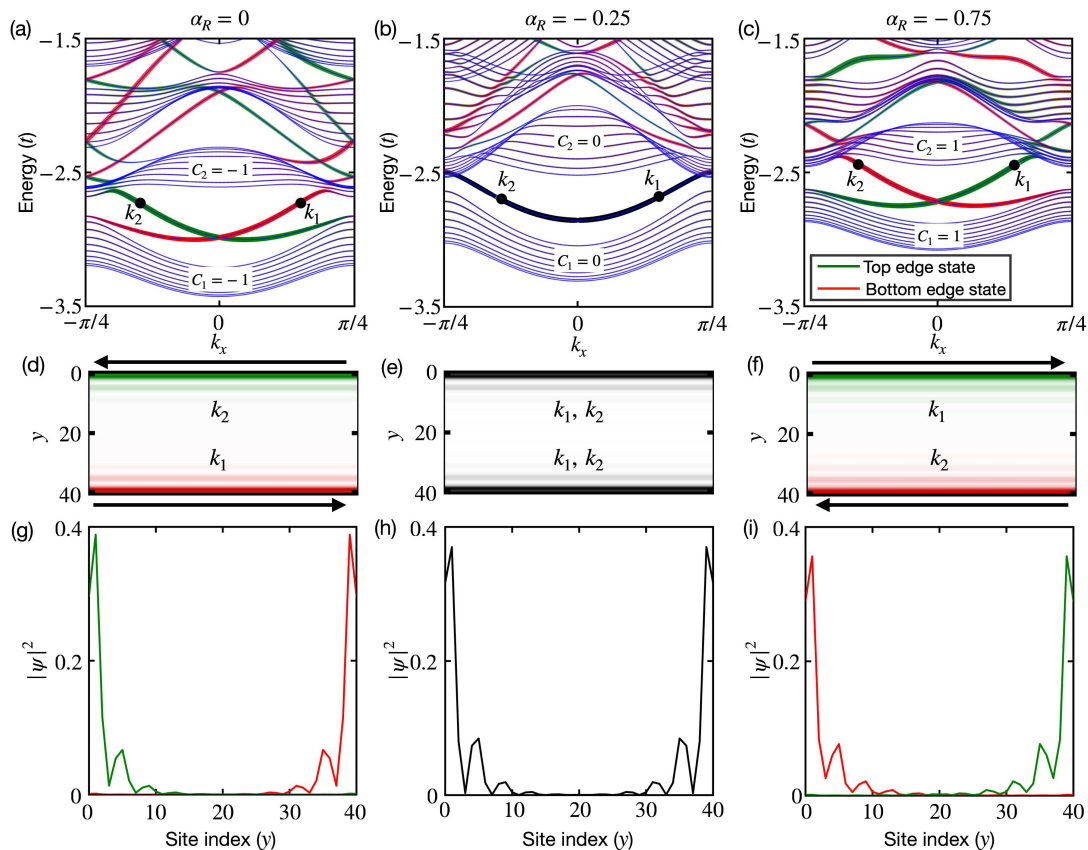


FIG. 6. Edge states for the nanoribbon geometry for three different  $\alpha_R$ : (a)  $\alpha_R = 0$ , (b)  $\alpha_R = -0.25$ , (c)  $\alpha_R = -0.75$ . The band topology for the three  $\alpha_R$  are different, as indicated from the Chern numbers of the lowest two subbands, which vary between -1, 0, and +1 for the three cases shown. The ribbon width is finite along the  $y$  direction (40 lattice sites corresponding to 10 magnetic unit cells), while its length is infinite along  $x$ . The middle panel shows the localization of the edge states either on the top edge or the bottom edge of the ribbon, and the color density is proportional to the wave function character  $|\psi(k)|^2$  for the edge states, which are labelled  $k_1$  and  $k_2$  in the top panel. The color coding, red or green, corresponds to localization along the bottom edge or the top edge of the ribbon, respectively, while the long arrows indicate the direction of propagation of the edge states. The bottom panel shows the wave function characters of the same edge states, which exponentially decay into the bulk. For  $\alpha_R = -0.25$ , the two midgap states at each  $k$  point are degenerate, corresponding to a state on the bottom edge and a state on the top edge, and constitute ordinary surface states with no topological character. They are shown in black colors in (b), (e), and (h).

ment, as seen in the case of quantum Hall effect (see Figure 3(b)).

Not only the band dispersion is modified due to the presence of Rashba SOC, but the topology of the band structure is also altered, leading to a change in the Chern numbers. The Chern numbers still remain integers for the isolated individual subbands, but their magnitudes change as one varies the strength  $\alpha_R$  of the Rashba SOC term. The results are shown for the  $4 \times 4$  square lattice in Figure 5 (a) for the lowest two subbands, where we see that the Chern numbers flip flop between the values  $\pm 2$  for the range of  $\alpha_R$  considered. Figure 5 (b-d) show the band structures as one passes through one of the crossover points, where the Chern number changes abruptly. The corresponding Berry curvatures are also shown in the Figure for  $\alpha_R$  slightly below and above this crossover value. In essence, the change in the band

topology occurs due to the changed magnetic field profile caused by the Rashba SOC term.

*Nanoribbon states.* The varying nature of the band topology (Chern numbers) with changing  $\alpha_R$  shows up in the edge states of the skyrmion crystal. We have computed the band structure in the nanoribbon geometry, where the ribbon is extended in the  $x$  direction, while it has a finite width along the  $y$  direction. The results are shown in Fig. 6 for three cases of  $\alpha_R$ . In particular, we focus on the lowest two bands and the edge states that occur in the midgap region between the two bands. The Chern numbers for the two lowest bulk subbands change from  $C = -1$  to 0 to +1, as indicated in the top panel. The top panel also shows the edge states which are color coded red/green, corresponding to states localized on the bottom/top edge of the ribbon as seen from the middle panel of the figure. As the Chern numbers change from

-1 to +1, the direction of propagation of the edge state is reversed, which is indicated by the long arrows in the middle panel of the Figure. For the case of  $\alpha_R = -0.25$ , Fig. 6(b), the lowest bulk bands are not topological in nature with zero Chern numbers, and the two edge states are degenerate in energy and constitute ordinary bound states.

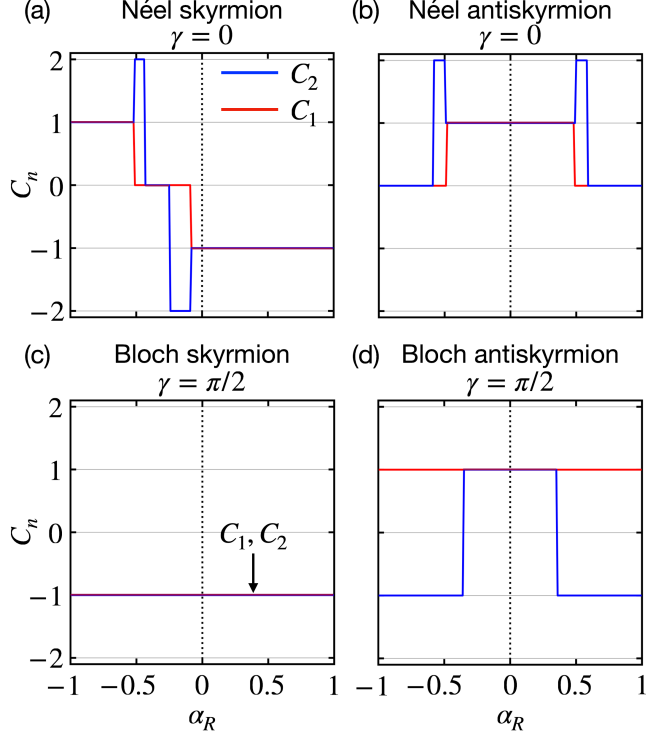


FIG. 7. Variation of the Chern numbers for the lowest two bands for four types of the skyrmion crystal as the Rashba SOC strength  $\alpha_R$  is changed.

*Band topology.* The Chern numbers of the individual subbands change at the strength of the Rashba SOC  $\alpha_R$  is varied, but always remaining an integer. The computed Chern numbers for the lowest two bands for four skyrmion types are shown in Fig. 7. The change in the Chern numbers is related to the change in the emergent magnetic field with  $\alpha_R$ . Except for the Néel skyrmion case, the Chern numbers are symmetric with respect to the change of the sign of  $\alpha_R$ , which can be understood in terms of the emergent magnetic fields, Eqs. (5-6), and the symmetry of the square lattice as discussed below.

(1) For the case of Bloch skyrmion (with ) helicity  $\gamma = \pi/2$ ), the Chern numbers do not change with  $\alpha_R$  as seen from Fig. 7 (c), since the  $\cos \gamma = 0$  factor in the magnetic field expression Eq. (5) removes any magnetic field dependence of  $\alpha_R$ .

(2) For the antiskyrmions with any helicity, the Chern numbers are independent of the sign of  $\alpha_R$  as seen from Figure 7 (b) and (d). This is because irrespective of the helicity for the antiskyrmions, the magnetic field, Eq. (6), is a  $90^\circ$  rotation of each other when the sign of  $\alpha_R$  is

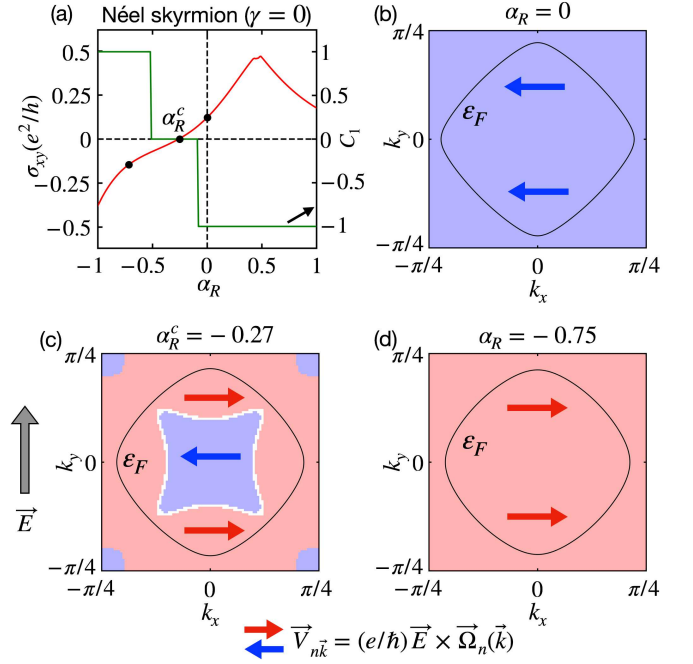


FIG. 8. THC in the presence of the Rashba SOC term for the lowest subband. (a) The green line shows the quantized Chern number for the *completely* filled lowest subband ( $C_1$ ) as a function of  $\alpha_R$ , which switches between zero and  $\pm 1$ , leading to a quantized THC,  $\sigma_{xy} = -e^2/h \times C_1$ . The red line shows the THC for the *half-filled* lowest subband indicating that it can be continuously tuned including a sign reversal at the cross over value  $\alpha_R^c$ . (b)-(d) Berry curvatures  $\Omega^z(\mathbf{k})$  in the Brillouin zone for three different values of  $\alpha_R$  (corresponding to the three black dots in (a)) showing positive (red) and negative (blue) regions of  $\Omega^z(\mathbf{k})$ . The blue/red arrows show the anomalous velocities  $e\hbar^{-1} \mathbf{E} \times \Omega^z(\mathbf{k})$  for the blue/red regions (color coded). The THC, which is the sum of  $\Omega^z(\mathbf{k})$  over the occupied states, becomes zero for  $\alpha_R^c \approx -0.27$  (Figure (c)) as the positive Berry curvature part cancels the negative part. The circles indicate the Fermi surface in each case.

reversed due to the  $\cos(2\alpha - \gamma)$  factor, while the square lattice has the same four-fold symmetry as well.

(3) Unlike antiskyrmions, for the case of skyrmions, the Chern numbers for  $\pm\alpha_R$  are not symmetric in general. This is because as Eq. (5) shows, the magnetic fields for  $\pm\alpha_R$  are different and unrelated by any symmetry. An exception is the trivial case of  $\cos \gamma = 0$ , where the Rashba contribution to the magnetic field Eq. (5) is zero, which makes the Chern numbers entirely independent of  $\alpha_R$ , as seen from Fig. 7 (c).

(4) Of the eight skyrmion types we have considered in this paper, Fig. 7 shows the Chern numbers only for the four cases. The other four cases in Figure 2 can be obtained from these results as well. Also, all properties for the Weyl SOC and Dresselhaus SOC including the subband Chern numbers can be expressed in terms of the results for the Rashba SOC as discussed later in the paper in Section V.

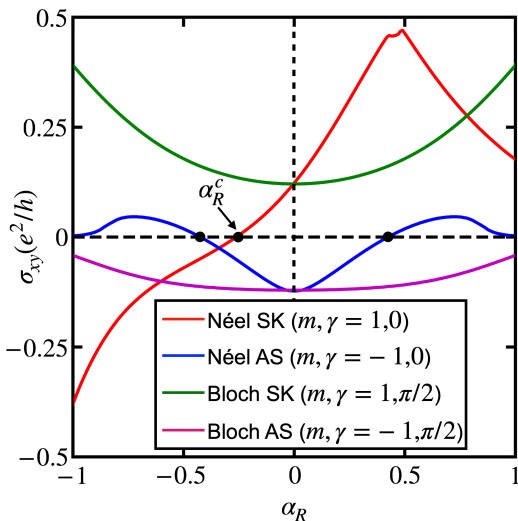


FIG. 9. Variation of  $\sigma_{xy}$  with the Rashba SOC strength  $\alpha_R$  for four different skyrmion types, with  $\sigma_{m,\gamma}$  denoting the four cases, where  $m$  is the vorticity and  $\gamma$  is the helicity. Here, the lowest subband is half-filled, but similar results are obtained for any partially-filled case. For completely filled subbands,  $\sigma_{xy}$  changes abruptly as shown in Figure 7. For the Néel skyrmion and antiskyrmion, there is a sign reversal in  $\sigma_{xy}$ , where changing  $\alpha_R$  through the crossover value  $\alpha_R^c$  changes its sign, so that the Hall current reverses in sign as illustrated in Figure 1. The crossover points are indicated by black dots.

#### IV. TOPOLOGICAL HALL EFFECT WITH PARTIALLY FILLED SUBBANDS

The abrupt change of the Chern numbers with  $\alpha_R$  leads to the quantized THC for the case of completely filled subbands. For the partially filled subbands, one gets a continuous change of the THC and the remarkable result that the sign of the THC can be flipped by a small change in  $\alpha_R$ . We illustrate this here for the case where the lowest subband is half filled.

The computed  $\sigma$  with the lowest subband half filled is shown in Fig. 8(a) as a function of  $\alpha_R$  for the Néel skyrmion, which shows a change of sign as  $\alpha_R$  varies through the crossover point  $\alpha_R \approx -0.27$ . This leads to the remarkable result that an applied electric field can reverse the polarity of the Hall current by tuning  $\alpha_R$ .

The results can be understood in terms of the change in the Berry curvatures as  $\alpha_R$  is varied. When  $\alpha_R$  is varied from the value -0.75 to zero, the Chern number of the lowest subband changes from  $C_1 = 1$  to  $C_1 = -1$ , which results in the Berry curvature  $\Omega_1^z(\mathbf{k})$  changing from a positive value to a negative value over the entire Brillouin zone as seen from Figure 8 (b) and (d). For intermediate values of  $\alpha_R$ , the positive regions slowly change into negative regions and at the crossover point, they exactly cancel each other and the THC  $\sigma$ , which is the sum of the Berry curvature over the occupied states, becomes zero.

We have studied the THC for the other skyrmion types as well. The results are shown in Figure 9. A similar sign

change of  $\sigma$  is seen for the Néel antiskyrmion. For the case of the Bloch skyrmion, the Rashba SOC term does not affect the magnetic field (see Eq. (5)) and as a result the Chern number for the lowest subbands remain always -1. There is no change of sign for  $\sigma$  in this case. For the case of the Bloch antiskyrmion, there is no polarity change within the range of  $\alpha_R$  values shown in Figure 9, but may happen when Figure 9 is larger.

#### V. DRESSELHAUS AND WEYL SOC

Apart from the Rashba SOC, one could also have a Dresselhaus or a Weyl type of SOC. While the Rashba SOC arises at the solid surface due to the surface inversion asymmetry and can be induced by an applied electric field, the Dresselhaus SOC arises due to the bulk inversion asymmetry. However, it has been demonstrated that the Dresselhaus SOC can be introduced and tuned in the 2D systems via interface engineering [57]. Furthermore, it has been recently pointed out that depending on the crystalline symmetry of the underlying material, it is possible to have Rashba, Dresselhaus, or Weyl type SOC, even at the  $\Gamma$  point of the Brillouin zone[60]. In view of this, for the sake of completeness, we also consider the effect of the Dresselhaus and Weyl type SOC. The SOC terms for these cases are written in momentum space as  $\mathcal{H}_{D/W}^{\text{SOC}} = \alpha_{D/W}(\sigma_x k_x \mp \sigma_y k_y)$  with the corresponding lattice version in real space  $\mathcal{H}_{D/W}^{\text{SOC}} = i\alpha_{D/W} \sum_{\langle ij \rangle} c_i^\dagger (\sigma_x r_{ij}^x \mp \sigma_y r_{ij}^y) c_j + H.c.$ , where the  $-(+)$  sign corresponds to the Dresselhaus (Weyl) SOC. The full Hamiltonians corresponding to Eq. (3) for the Rashba case read

$$\begin{aligned} \mathcal{H}_D = & -t \sum_{\langle ij \rangle} \cos \frac{\theta_{ij}}{2} e^{ia_{ij}} d_i^\dagger d_j \\ & - i\alpha_D \sum_{\langle ij \rangle} [e^{i\phi_j} (r_{ij}^x + ir_{ij}^y) \cos \frac{\theta_i}{2} \sin \frac{\theta_j}{2} \\ & + e^{-i\phi_i} (r_{ij}^x - ir_{ij}^y) \cos \frac{\theta_j}{2} \sin \frac{\theta_i}{2}] d_i^\dagger d_j + H.c. \end{aligned} \quad (12)$$

$$\begin{aligned} \mathcal{H}_W = & -t \sum_{\langle ij \rangle} \cos \frac{\theta_{ij}}{2} e^{ia_{ij}} d_i^\dagger d_j \\ & - i\alpha_W \sum_{\langle ij \rangle} [e^{i\phi_j} (r_{ij}^x - ir_{ij}^y) \cos \frac{\theta_i}{2} \sin \frac{\theta_j}{2} \\ & + e^{-i\phi_i} (r_{ij}^x + ir_{ij}^y) \cos \frac{\theta_j}{2} \sin \frac{\theta_i}{2}] d_i^\dagger d_j + H.c. \end{aligned} \quad (13)$$

where again  $d, d^\dagger$  are the spinless fermion operators as before, since we are taking  $J \rightarrow \infty$ .

As for the Rashba case, the net magnetic field seen by the electron may be determined by taking an infinitesimal square loop around a spatial point and computing the flux through it from the Peierls phase accumulated by



TABLE I. THC in the presence of Dresselhaus and Weyl SOC, expressed in terms of the THC for the Rashba SOC, with  $\alpha$  being the SOC strength in each case. As the Table shows, the THC for all cases can be expressed in terms of just four conductivities, viz.,  $\sigma_{1,0}(\alpha)$ ,  $\sigma_{-1,0}(\alpha)$ ,  $\sigma_{1,\pi/2}(\alpha)$ , and  $\sigma_{-1,\pi/2}(\alpha)$ , where  $\sigma_{m,\gamma}(\alpha) \equiv \sigma_{m,\gamma}^R(\alpha)$  is the THC with Rashba SOC. For example, the table shows that  $\sigma_{1,0}^W(\alpha) = \sigma_{1,\pi/2}^R(-\alpha)$ , which is the first result listed under Weyl. The four independent conductivities have been plotted in Fig. 9 for the case when the lowest subband is half-filled. However, the correspondence is valid for any filling, whether we have completely filled or partially filled subbands.

| Skyrmion type            |          | Rashba                        | Dresselhaus                   | Weyl                          |                              |
|--------------------------|----------|-------------------------------|-------------------------------|-------------------------------|------------------------------|
| Vorticity                | Helicity | $\sigma_{m,\gamma}^R(\alpha)$ | $\sigma_{m,\gamma}^D(\alpha)$ | $\sigma_{m,\gamma}^W(\alpha)$ |                              |
| skyrmion<br>$m = 1$      | Néel     | $\gamma = 0$                  | $\sigma_{1,0}(\alpha)$        | $-\sigma_{-1,\pi/2}(\alpha)$  | $\sigma_{1,\pi/2}(-\alpha)$  |
|                          |          | $\gamma = \pi$                | $\sigma_{1,0}(-\alpha)$       | $-\sigma_{-1,\pi/2}(-\alpha)$ | $\sigma_{1,\pi/2}(\alpha)$   |
|                          | Bloch    | $\gamma = \pi/2$              | $\sigma_{1,\pi/2}(\alpha)$    | $-\sigma_{-1,0}(\alpha)$      | $\sigma_{1,0}(\alpha)$       |
|                          |          | $\gamma = -\pi/2$             | $\sigma_{1,\pi/2}(-\alpha)$   | $-\sigma_{-1,0}(-\alpha)$     | $\sigma_{1,0}(-\alpha)$      |
| antiskyrmion<br>$m = -1$ | Néel     | $\gamma = 0$                  | $\sigma_{-1,0}(\alpha)$       | $-\sigma_{1,\pi/2}(\alpha)$   | $\sigma_{-1,\pi/2}(-\alpha)$ |
|                          |          | $\gamma = \pi$                | $\sigma_{-1,0}(-\alpha)$      | $-\sigma_{1,\pi/2}(-\alpha)$  | $\sigma_{-1,\pi/2}(\alpha)$  |
|                          | Bloch    | $\gamma = \pi/2$              | $\sigma_{-1,\pi/2}(\alpha)$   | $-\sigma_{1,0}(\alpha)$       | $\sigma_{-1,0}(\alpha)$      |
|                          |          | $\gamma = -\pi/2$             | $\sigma_{-1,\pi/2}(-\alpha)$  | $-\sigma_{1,0}(-\alpha)$      | $\sigma_{-1,0}(-\alpha)$     |

the electron while traveling around the loop. The results are:

$$B_{SK}^D(r, \alpha) = \frac{\pi}{2\lambda r} \sin \frac{\pi r}{\lambda} + \frac{\alpha_R}{t} \left( \frac{\pi}{\lambda} \cos \frac{\pi r}{\lambda} - \frac{1}{r} \sin \frac{\pi r}{\lambda} \right) \sin(2\alpha + \gamma), \quad (\text{Dresselhaus/skyrmion}) \quad (14)$$

$$B_{AS}^D(r) = -\frac{\pi}{2\lambda r} \sin \frac{\pi r}{\lambda} + \frac{\alpha_R}{t} \left( \frac{\pi}{\lambda} \cos \frac{\pi r}{\lambda} + \frac{1}{r} \sin \frac{\pi r}{\lambda} \right) \sin \gamma, \quad (\text{Dresselhaus/antiskyrmion}) \quad (15)$$

$$B_{SK}^W(r) = \frac{\pi}{2\lambda r} \sin \frac{\pi r}{\lambda} - \frac{\alpha_R}{t} \left( \frac{\pi}{\lambda} \cos \frac{\pi r}{\lambda} + \frac{1}{r} \sin \frac{\pi r}{\lambda} \right) \sin \gamma, \quad (\text{Weyl/skyrmion}) \quad (16)$$

$$B_{AS}^W(r, \alpha) = -\frac{\pi}{2\lambda r} \sin \frac{\pi r}{\lambda} - \frac{\alpha_R}{t} \left( \frac{\pi}{\lambda} \cos \frac{\pi r}{\lambda} - \frac{1}{r} \sin \frac{\pi r}{\lambda} \right) \sin(\gamma - 2\alpha), \quad (\text{Weyl/antiskyrmion}) \quad (17)$$

for  $r < \lambda$  and zero otherwise. The magnetic fields are in units of  $\Phi_0/(2\pi)$ , where  $\phi_0$  is the flux quantum.

It turns out that the Hamiltonian for the three cases of SOC (Rashba SOC, Dresselhaus SOC, or Weyl SOC) can be mapped into one another for the skyrmion types considered in the paper. As a result, the various physical quantities, in particular, the emergent magnetic fields as well as the THC are related to one another. The THC's can be expressed, as summarized in Table I, in terms of just four quantities, viz.,  $\sigma_{1,0}(\alpha)$ ,  $\sigma_{-1,0}$ ,  $\sigma_{1,\pi/2}$ , and  $\sigma_{-1,\pi/2}$ , where  $\sigma_{m,\gamma}$  is the THC in the presence of the Rashba SOC, with  $m, \gamma$  being the vorticity and the helicity, respectively. These relations can be understood by noting the following points:

(1) For the THC in two cases to be the same, one must check that the emergent magnetic fields are the same, which is a necessary condition. However, this is not sufficient, since the effective hopping magnitude between two lattice sites can still be different even though the magnetic fields are the same. As an example, con-

sidering the THC  $\sigma_{1,\pi/2}$  for the Rashba SOC case (green curve in Fig. 9), the magnetic field is independent of the Rashba SOC strength  $\alpha_R$  due to the  $\cos \gamma = 0$  factor (see Eq. (5)). Nevertheless, the THC does change with  $\alpha_R$  because the hopping amplitudes between two sites are functions of both  $t$  and  $\alpha_R$ .

(2) The Hamiltonians possess certain symmetries. It is easy to see that in all three cases  $\mathcal{H}_R$ ,  $\mathcal{H}_D$ , and  $\mathcal{H}_W$  (Eqs. (3), (12), and (13)), when the sign of the SOC strength  $\alpha$  is flipped and the helicity  $m$  is changed by  $\pi$  simultaneously, the Hamiltonian remains unchanged. This leads to identical band structures and all other electronic properties including transport, so that we have the equality:  $\sigma_{m,\gamma}^X(\alpha) = \sigma_{m,\gamma \pm \pi}^X(-\alpha)$ , where  $X = R, D$ , or  $W$ .

(3) The Weyl Hamiltonian for a certain skyrmion type turns out to be the same as the Rashba Hamiltonian for certain other skyrmion type. For example, if we compare the Rashba Hamiltonian for the Néel skyrmion ( $m = 1, \gamma = 0$ ) and the Weyl Hamiltonian for the Bloch skyrmion ( $m = 1, \gamma = \pi/2$ ), it is easily shown from Eqs.

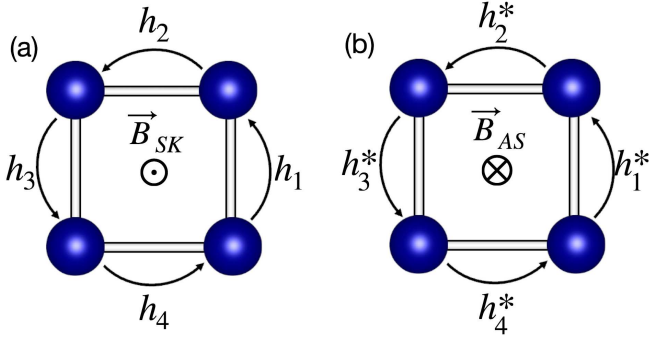


FIG. 10. Equivalence of the Hamiltonians in the skyrmion crystal between the two cases: (a) Néel skyrmion with  $\gamma = 0$  in the presence of Rashba SOC and (b) Bloch antiskyrmion with  $\gamma = \pi/2$  in the presence of Dresselhaus SOC. As discussed in the text, the effective hopping  $h_{ij}$  (denoted in the figure by  $h_n$ ), which includes both the direct hopping and the SOC term, is complex conjugate between the two cases. Thus, the emergent magnetic fields are the same but in the opposite directions as shown, which in turn leads to the THC, which are of the same magnitude but opposite signs between the two cases.

(3) and (13) that the two Hamiltonians are identical (see Supplementary Materials for details). Thus, we have  $\sigma_{1,\pi/2}^W(\alpha) = \sigma_{1,0}^R(\alpha)$ . There are several other such equalities, which have been used to construct Table I. These have been explicitly verified by computing the THC's for both cases.

(4) The Rashba and Dresselhaus Hamiltonians with certain skyrmion types are related to each other via a complex conjugate hopping. For instance, considering the two cases: (i) Rashba Hamiltonian for the Néel skyrmion ( $m = 1, \gamma = 0$ ) and (ii) Dresselhaus Hamiltonian for the Bloch antiskyrmion ( $m = -1, \gamma = \pi/2$ ), it is easily shown from Eqs. (3) and (12) that all terms of the two Hamiltonians are the same except that the coefficients are complex conjugate of each other as illustrated in Figure 10 ( $h_{ij}d_j^\dagger d_i$  in one case vs.  $h_{ij}^*d_j^\dagger d_i$  for the other case, mathematical expressions are given in Supplementary Materials). This means that the effective magnetic fields that the electron sees as it hops from one site to another are simply of the opposite signs. This in turn implies that the two THC's are negative of each other, because if two magnetic fields are applied to the same system in opposite directions, the sum of the two Hall conductivities must add up to zero. This leads to the equality  $\sigma_{-1,\pi/2}^D(\alpha) = -\sigma_{1,0}^R(\alpha)$ . Similarly, several other correspondences between the Rashba and Dresselhaus conductivities are found, which are used to produce Table I.

## VI. SUMMARY

In summary, we presented a comprehensive analysis of the topological Hall effect in the skyrmion crystal in the presence of spin-orbit coupling, of Rashba, Dresselhaus, or the Weyl type. We considered the square lattice as a prototype and the magnetic unit cell contained a skyrmion or an antiskyrmion of either Bloch or Néel type. Detail results for the band structure and the THC were presented for the Rashba SOC, and we showed that the results for the other two cases (Dresselhaus SOC and Weyl SOC) can be expressed in terms of the Rashba results.

The presence of the SOC term affects the electron motion in two ways. First, it modifies the emergent magnetic field seen by the electron as it moves from site to site, and second, the hopping amplitudes are also modified (see Supplementary Materials for a concrete example). While both affect the band dispersion and the THC, the first term modifies the band topology (Chern numbers) as well.

Expressions for the emergent magnetic field were obtained for the isolated skyrmion or antiskyrmion in the presence of all three SOC terms. These results are useful in the interpretation of the electronic band structure and the THC in the skyrmion crystal. The competition between the emerging magnetic field due to the skyrmion texture and the SOC term leads to a tuning of the band dispersion and, therefore, the magnitude of the THC in any type of skyrmion. For example, for the Rashba SOC case and the Néel skyrmion crystal, we showed that for a critical value  $\alpha_R^0$  of the SOC strength, the combined magnetic field due to the skyrmion and the SOC term is uniform enough to produce the band structure similar to that in a uniform magnetic field, leading to prominent Hall plateaus.

We found that the band topology, e.g., the subband Chern numbers, can be changed by varying the strength of the SOC. The detail behavior depends on the type of the skyrmion (vorticity and helicity) as well as the type of the SOC (Rashba, Dresselhaus, or Weyl). The change in the band topology shows up in the topological nature of the edge states. An interesting effect is that the direction of the edge current can be reversed by changing the strength of the SOC.

For partially filled subbands, the change in the band topology with the SOC strength results in the tuning of the THC. Not only its magnitude can be changed, but even the sign can be reversed in some cases, so that the direction of the Hall current flips. Explicit results were presented for Rashba SOC, where the sign flip occurs for the Néel skyrmion or antiskyrmion, but not for the Bloch case. The sign flip was explained from the momentum-space Berry curvatures, which changes gradually from everywhere positive in the Brillouin zone to everywhere negative as the Rashba SOC strength is varied, so that at the crossover point  $\alpha_R^c$ , the negative and positive portions of the Berry curvatures in the Brillouin zone add

up to zero, and the sign of the THC flips. This also happens for the Dresselhaus SOC and Weyl SOC, though for different types of skyrmions, which can be inferred from the mapping presented in Table I.

We showed that the results for the Dresselhaus SOC and Weyl SOC can be mapped into the case for Rashba SOC, because the Hamiltonians are either the same or they are related by symmetry. Keeping this in mind, we have discussed the Rashba SOC case in detail. Results for the Dresselhaus SOC and Weyl SOC cases, including the THC, can be inferred from the appropriate mapping, which are summarized in Table I.

Experimenters are increasingly successful in fabricating skyrmions crystals, even though their stability and manipulation hinge on a delicate interplay between magnetic interactions, external fields, and temperature. It is also well established that the strength of the Rashba SOC can be tuned via an external electric field, and also in some cases, experimenters have been able to gener-

ate and tune the Dresselhaus SOC via interface engineering. These developments on the experimental front allow for the study of the many interesting phenomena predicted here for the skyrmion crystal including the tuning of the band topology and the THC, as well as the sign reversal of the Hall current and the edge current in the nanoribbons. This could lead to a fertile playground for skyrmion-based spintronics applications.

## VII. ACKNOWLEDGEMENTS

This work is funded by the Department of Science and Technology, India, through Grant No. CRG/2020/004330. AM thanks MoE India for the PMRF fellowship. SS thanks SERB India for the VA-JRA fellowship.

- 
- [1] T. Skyrme, A unified field theory of mesons and baryons, *Nuclear Physics* **31**, 556 (1962).
- [2] A. N. Bogdanov and D. A. Yablonskii, Thermodynamically stable “vortices” in magnetically ordered crystals: the mixed state of magnets, *Soviet Phys. JETP* **68**, 101 (1989).
- [3] A. Bogdanov, M. Kudinov, and D. Yablonskii, Theory of magnetic vortices in easy-axis ferromagnets, *Soviet Phys. Solid State* **31** (1989).
- [4] C. Back, V. Cros, H. Ebert, K. Everschor-Sitte, A. Fert, M. Garst, T. Ma, S. Mankovsky, T. L. Monchesky, M. Mostovoy, N. Nagaosa, S. S. P. Parkin, C. Pfleiderer, N. Reyren, A. Rosch, Y. Taguchi, Y. Tokura, K. von Bergmann, and J. Zang, The 2020 skyrmionics roadmap, *Journal of Physics D: Applied Physics* **53**, 363001 (2020).
- [5] A. Fert, V. Cros, and J. Sampaio, Skyrmions on the track, *Nature Nanotechnology* **8**, 152 (2013).
- [6] N. Nagaosa and Y. Tokura, Topological properties and dynamics of magnetic skyrmions, *Nature Nanotechnology* **8**, 899 (2013).
- [7] Y. Tokura and N. Kanazawa, Magnetic skyrmion materials, *Chemical Reviews* **121**, 2857 (2021).
- [8] B. Göbel, I. Mertig, and O. A. Tretiakov, Beyond skyrmions: Review and perspectives of alternative magnetic quasiparticles, *Physics Reports* **895**, 1 (2021), beyond skyrmions: Review and perspectives of alternative magnetic quasiparticles.
- [9] S. Bhowal, S. Satpathy, and P. Sahu, Magnetic skyrmions in condensed matter physics, *Student J. Phys.* **8**, arXiv:2005.07635v1 (2020).
- [10] T.-L. Ho, Spinor Bose condensates in optical traps, *Phys. Rev. Lett.* **81**, 742 (1998).
- [11] T. Ohmi and K. Machida, Bose-Einstein condensation with internal degrees of freedom in alkali atom gases, *Journal of the Physical Society of Japan* **67**, 1822 (1998).
- [12] D. C. Wright and N. D. Mermin, Crystalline liquids: the blue phases, *Rev. Mod. Phys.* **61**, 385 (1989).
- [13] M. Abolfath, J. J. Palacios, H. A. Fertig, S. M. Girvin, and A. H. MacDonald, Critical comparison of classical field theory and microscopic wave functions for skyrmions in quantum Hall ferromagnets, *Phys. Rev. B* **56**, 6795 (1997).
- [14] S. L. Sondhi, A. Karlhede, S. A. Kivelson, and E. H. Rezayi, Skyrmions and the crossover from the integer to fractional quantum Hall effect at small Zeeman energies, *Phys. Rev. B* **47**, 16419 (1993).
- [15] A. Bogdanov and A. Hubert, Thermodynamically stable magnetic vortex states in magnetic crystals, *Journal of Magnetism and Magnetic Materials* **138**, 255 (1994).
- [16] S. Mühlbauer, B. Binz, F. Jonietz, C. Pfleiderer, A. Rosch, A. Neubauer, R. Georgii, and P. Böni, Skyrmion lattice in a chiral magnet, *Science* **323**, 915 (2009).
- [17] B. Lebech, J. Bernhard, and T. Freltoft, Magnetic structures of cubic fcc studied by small-angle neutron scattering, *Journal of Physics: Condensed Matter* **1**, 6105 (1989).
- [18] J. Matsuno, N. Ogawa, K. Yasuda, F. Kagawa, W. Koshibae, N. Nagaosa, Y. Tokura, and M. Kawasaki, Interface-driven topological Hall effect in SrRuO<sub>3</sub> – SrIrO<sub>3</sub> bilayer, *Science Advances* **2**, e1600304 (2016), <https://www.science.org/doi/pdf/10.1126/sciadv.1600304>.
- [19] L. Wang, Q. Feng, Y. Kim, R. Kim, K. H. Lee, S. D. Pollard, Y. J. Shin, H. Zhou, W. Peng, D. Lee, W. Meng, H. Yang, J. H. Han, M. Kim, Q. Lu, and T. W. Noh, Ferroelectrically tunable magnetic skyrmions in ultrathin oxide heterostructures, *Nature Materials* **17**, 1087 (2018).
- [20] C. Felser and S. Parkin, Topology, skyrmions, and Heusler compounds, *MRS Bulletin* **47**, 600 (2022).
- [21] J. Jiang and W. Mi, Two-dimensional magnetic Janus monolayers and their van der Waals heterostructures: a review on recent progress, *Mater. Horiz.* **10**, 788 (2023).
- [22] W. Sun, W. Wang, C. Yang, X. Li, H. Li, S. Huang, and Z. Cheng, Quantized movement of magnetic skyrmions in moiré multiferroic heterostructures, *Phys. Rev. B* **107**, 184439 (2023).

- [23] T. Kurumaji, T. Nakajima, M. Hirschberger, A. Kikkawa, Y. Yamasaki, H. Sagayama, H. Nakao, Y. Taguchi, T. hisa Arima, and Y. Tokura, Skyrmion lattice with a giant topological Hall effect in a frustrated triangular-lattice magnet, *Science* **365**, 914 (2019), <https://www.science.org/doi/pdf/10.1126/science.aau0968>.
- [24] S. Heinze, K. von Bergmann, M. Menzel, J. Brede, A. Kubetzka, R. Wiesendanger, G. Bihlmayer, and S. Blügel, Spontaneous atomic-scale magnetic skyrmion lattice in two dimensions, *Nature Physics* **7**, 713 (2011).
- [25] U. K. Rößler, A. N. Bogdanov, and C. Pfleiderer, Spontaneous skyrmion ground states in magnetic metals, *Nature* **442**, 797 (2006).
- [26] L. Brey, H. A. Fertig, R. Côté, and A. H. MacDonald, Skyrme crystal in a two-dimensional electron gas, *Phys. Rev. Lett.* **75**, 2562 (1995).
- [27] A. Bogdanov and A. Hubert, Thermodynamically stable magnetic vortex states in magnetic crystals, *Journal of Magnetism and Magnetic Materials* **138**, 255 (1994).
- [28] T. Okubo, S. Chung, and H. Kawamura, Multiple- $q$  states and the skyrmion lattice of the triangular-lattice heisenberg antiferromagnet under magnetic fields, *Phys. Rev. Lett.* **108**, 017206 (2012).
- [29] A. O. Leonov and M. Mostovoy, Multiply periodic states and isolated skyrmions in an anisotropic frustrated magnet, *Nature Communications* **6**, 8275 (2015).
- [30] T. Gorkan, J. Das, J. Kapeghian, M. Akram, J. V. Barth, S. Tongay, E. Akturk, O. Erten, and A. S. Botana, Skyrmion formation in Ni-based Janus dihalide monolayers: Interplay between magnetic frustration and Dzyaloshinskii-Moriya interaction, *Phys. Rev. Mater.* **7**, 054006 (2023).
- [31] D. Amoroso, P. Barone, and S. Picozzi, Spontaneous skyrmionic lattice from anisotropic symmetric exchange in a Ni-halide monolayer, *Nature Communications* **11**, 5784 (2020).
- [32] S. Hayami and Y. Motome, Square skyrmion crystal in centrosymmetric itinerant magnets, *Phys. Rev. B* **103**, 024439 (2021).
- [33] S. Hayami, Skyrmion crystal induced by four-spin interactions in itinerant triangular magnets, *Magnetism* **4**, 281 (2024).
- [34] S. Paul, S. Halder, S. von Malottki, and S. Heinze, Role of higher-order exchange interactions for skyrmion stability, *Nature Communications* **11**, 4756 (2020).
- [35] X.-C. Hu, H.-T. Wu, and X. R. Wang, A theory of skyrmion crystal formation, *Nanoscale* **14**, 7516 (2022).
- [36] W. Münzer, A. Neubauer, T. Adams, S. Mühlbauer, C. Franz, F. Jonietz, R. Georgii, P. Böni, B. Pedersen, M. Schmidt, A. Rosch, and C. Pfleiderer, Skyrmion lattice in the doped semiconductor  $\text{Fe}_{1-x}\text{Co}_x\text{Si}$ , *Phys. Rev. B* **81**, 041203 (2010).
- [37] X. Z. Yu, Y. Onose, N. Kanazawa, J. H. Park, J. H. Han, Y. Matsui, N. Nagaosa, and Y. Tokura, Real-space observation of a two-dimensional skyrmion crystal, *Nature* **465**, 901 (2010).
- [38] X. Z. Yu, N. Kanazawa, Y. Onose, K. Kimoto, W. Z. Zhang, S. Ishiwata, Y. Matsui, and Y. Tokura, Near room-temperature formation of a skyrmion crystal in thin-films of the helimagnet  $\text{FeGe}$ , *Nature Materials* **10**, 106 (2011).
- [39] T.-H. Kim, H. Zhao, B. Xu, B. A. Jensen, A. H. King, M. J. Kramer, C. Nan, L. Ke, and L. Zhou, Mechanisms of skyrmion and skyrmion crystal formation from the conical phase, *Nano Letters* **20**, 4731 (2020).
- [40] K. Karube, J. S. White, N. Reynolds, J. L. Gavilano, H. Oike, A. Kikkawa, F. Kagawa, Y. Tokunaga, H. M. Rønnow, Y. Tokura, and Y. Taguchi, Robust metastable skyrmions and their triangular-square lattice structural transition in a high-temperature chiral magnet, *Nature Materials* **15**, 1237 (2016).
- [41] T. Kurumaji, T. Nakajima, M. Hirschberger, A. Kikkawa, Y. Yamasaki, H. Sagayama, H. Nakao, Y. Taguchi, T. hisa Arima, and Y. Tokura, Skyrmion lattice with a giant topological Hall effect in a frustrated triangular-lattice magnet, *Science* **365**, 914 (2019), <https://www.science.org/doi/pdf/10.1126/science.aau0968>.
- [42] M. Hirschberger, T. Nakajima, S. Gao, L. Peng, A. Kikkawa, T. Kurumaji, M. Kriener, Y. Yamasaki, H. Sagayama, H. Nakao, K. Ohishi, K. Kakurai, Y. Taguchi, X. Yu, T.-h. Arima, and Y. Tokura, Skyrmion phase and competing magnetic orders on a breathing kagomé lattice, *Nature Communications* **10**, 5831 (2019).
- [43] S. Heinze, K. von Bergmann, M. Menzel, J. Brede, A. Kubetzka, R. Wiesendanger, G. Bihlmayer, and S. Blügel, Spontaneous atomic-scale magnetic skyrmion lattice in two dimensions, *Nature Physics* **7**, 713 (2011).
- [44] N. D. Khanh, T. Nakajima, X. Yu, S. Gao, K. Shibata, M. Hirschberger, Y. Yamasaki, H. Sagayama, H. Nakao, L. Peng, K. Nakajima, R. Takagi, T.-h. Arima, Y. Tokura, and S. Seki, Nanometric square skyrmion lattice in a centrosymmetric tetragonal magnet, *Nature Nanotechnology* **15**, 444 (2020).
- [45] R. Takagi, N. Matsuyama, V. Ukleev, L. Yu, J. S. White, S. Francoual, J. R. L. Mardegan, S. Hayami, H. Saito, K. Kaneko, K. Ohishi, Y. Onuki, T.-h. Arima, Y. Tokura, T. Nakajima, and S. Seki, Square and rhombic lattices of magnetic skyrmions in a centrosymmetric binary compound, *Nature Communications* **13**, 1472 (2022).
- [46] H. Wang, Y. Dai, G.-M. Chow, and J. Chen, Topological Hall transport: Materials, mechanisms and potential applications, *Progress in Materials Science* **130**, 100971 (2022).
- [47] Y. Ohuchi, J. Matsuno, N. Ogawa, Y. Kozuka, M. Uchida, Y. Tokura, and M. Kawasaki, Electric-field control of anomalous and topological Hall effects in oxide bilayer thin films, *Nature Communications* **9**, 213 (2018).
- [48] Y. Gu, Y.-W. Wei, K. Xu, H. Zhang, F. Wang, F. Li, M. S. Saleem, C.-Z. Chang, J. Sun, C. Song, J. Feng, X. Zhong, W. Liu, Z. Zhang, J. Zhu, and F. Pan, Interfacial oxygen-octahedral-tilting-driven electrically tunable topological Hall effect in ultrathin  $\text{SrRuO}_3$  films, *Journal of Physics D: Applied Physics* **52**, 404001 (2019).
- [49] Y. Zhang and C. Zhang, Quantized anomalous Hall insulator in a nanopatterned two-dimensional electron gas, *Phys. Rev. B* **84**, 085123 (2011).
- [50] C. L. Kane and E. J. Mele,  $\mathbb{Z}_2$  topological order and the quantum spin Hall effect, *Phys. Rev. Lett.* **95**, 146802 (2005).
- [51] K. V. Shanavas and S. Satpathy, Electric field tuning of the Rashba effect in the polar perovskite structures, *Phys. Rev. Lett.* **112**, 086802 (2014).
- [52] P. Sahu, B. R. K. Nanda, and S. Satpathy, Formation of the skyrmionic polaron by Rashba and Dresselhaus spin-orbit coupling, *Phys. Rev. B* **106**, 224403 (2022).

- [53] D. R. Hofstadter, Energy levels and wave functions of bloch electrons in rational and irrational magnetic fields, *Phys. Rev. B* **14**, 2239 (1976).
- [54] K. Hamamoto, M. Ezawa, and N. Nagaosa, Quantized topological Hall effect in skyrmion crystal, *Phys. Rev. B* **92**, 115417 (2015).
- [55] B. Göbel, A. Mook, J. Henk, and I. Mertig, Signatures of lattice geometry in quantum and topological Hall effect, *New Journal of Physics* **19**, 063042 (2017).
- [56] L. Onsager, Interpretation of the de Haas-van Alphen effect, *The London, Edinburgh, and Dublin Philosophical Magazine and Journal of Science* **75**, 433 (1963), <https://doi.org/10.1080/14786440908521019>.
- [57] J. Yu, X. Zeng, S. Cheng, Y. Chen, Y. Liu, Y. Lai, Q. Zheng, and J. Ren, Tuning of Rashba/Dresselhaus spin splittings by inserting ultra-thin InAs layers at interfaces in insulating GaAs/AlGaAs quantum wells, *Nanoscale Research Letters* **11**, 477 (2016).
- [58] Z. Scherübl, G. m. H. Fülöp, M. H. Madsen, J. Nygård, and S. Csonka, Electrical tuning of Rashba spin-orbit interaction in multigated InAs nanowires, *Phys. Rev. B* **94**, 035444 (2016).
- [59] M.-C. Chang and Q. Niu, Berry phase, hyperorbits, and the Hofstadter spectrum, *Journal of Science* **75**, 433 (1963).
- [60] C. Mera Acosta, L. Yuan, G. M. Dalpian, and A. Zunger, Different shapes of spin textures as a journey through the Brillouin zone, *Phys. Rev. B* **104**, 104408 (2021).

## VIII. SUPPLEMENTARY MATERIALS

### A. Spin-Orbit Coupling in momentum space vs. the lattice version

*Rashba SOC.* Here, we show that the lattice version of the Rashba spin-orbit coupling (SOC) Hamiltonian, which appears in Eq. (1) of the main text, leads to the familiar form for the Rashba term in the momentum space for the free electrons, viz.,

$$\mathcal{H}_R^k = \alpha'_R (\boldsymbol{\sigma} \times \mathbf{k}) \cdot \hat{z} = \alpha'_R (\sigma_x k_y - \sigma_y k_x). \quad (18)$$

From the main text Eq. (1), the lattice version of the Rashba Hamiltonian is

$$\mathcal{H}_R^l = -i\alpha_R \sum_{i,j} c_i^\dagger (\sigma_x r_{ij}^y - \sigma_y r_{ij}^x) c_j, \quad (19)$$

where again the spin indices have been suppressed on the fermion operators  $c_i^\dagger/c_j$ ,  $\boldsymbol{\sigma}$  is as usual the Pauli matrices, and  $\mathbf{r}_{ij} \equiv \mathbf{r}_j - \mathbf{r}_i$  is the distance vectors between the two sites. Taking the case of the square lattice, we show that the real space form Eq. (19) leads to the momentum space form Eq. (18) for small  $k$ .

Going to the momentum space with the Bloch function basis, the matrix elements of Eq. (19) become

$$\mathcal{H}_R^{l,\uparrow\uparrow} = 0, \quad (20)$$

$$\mathcal{H}_R^{l,\downarrow\downarrow} = 0, \quad (21)$$

$$\begin{aligned} \mathcal{H}_R^{l,\uparrow\downarrow} &= \alpha_R a (e^{ik_x a} - e^{-ik_x a}) - i\alpha_R a (e^{ik_y a} - e^{-ik_y a}) \\ &= 2\alpha_R a (\sin k_y a + i \sin k_x a), \end{aligned} \quad (22)$$

$$\begin{aligned} \mathcal{H}_R^{l,\downarrow\uparrow} &= -\alpha_R a (e^{ik_x a} - e^{-ik_x a}) - i\alpha_R a (e^{ik_y a} - e^{-ik_y a}) \\ &= 2\alpha_R a (\sin k_y a - i \sin k_x a), \end{aligned} \quad (23)$$

where  $a$  is the lattice constant. To get the free-electron case, we take the small momentum limit, which immediately yields the familiar form of the Rashba Hamiltonian

$$\mathcal{H}_R^k = \alpha'_R \begin{pmatrix} 0 & k_y + ik_x \\ k_y - ik_x & 0 \end{pmatrix} = \alpha'_R (\sigma_x k_y - \sigma_y k_x), \quad (24)$$

where  $\alpha'_R = 2\alpha_R a^2$ .

*Dresselhaus and Weyl SOC.* Proceeding in the same way, we easily see that for the Dresselhaus and Weyl SOC, the corresponding Hamiltonian forms are equivalent for small momentum  $k$ :

$$\mathcal{H}_D^k = \alpha'_D (\sigma_x k_x - \sigma_y k_y), \quad (25)$$

$$\mathcal{H}_D = -i\alpha_D \sum_{i,j} c_i^\dagger (\sigma_x r_{ij}^x - \sigma_y r_{ij}^y) c_j, \quad (26)$$

$$\mathcal{H}_W^k = \alpha'_W (\sigma_x k_x + \sigma_y k_y), \quad (27)$$

$$\mathcal{H}_W = -i\alpha_W \sum_{i,j} c_i^\dagger (\sigma_x r_{ij}^x + \sigma_y r_{ij}^y) c_j. \quad (28)$$

### B. Comparison Between square lattice under uniform magnetic field and skyrmion lattice with optimal Rashba SOC

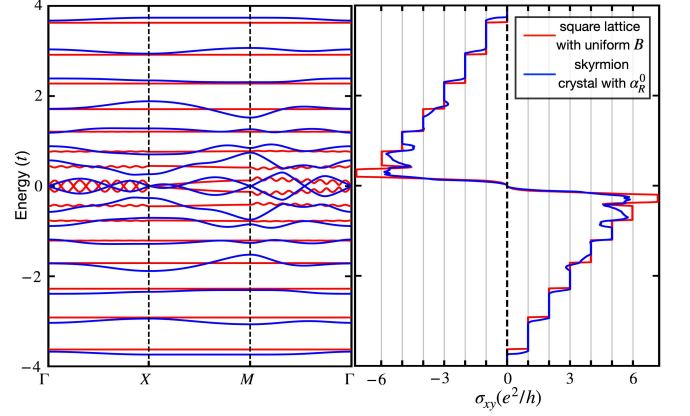


FIG. 11. Red lines show the band structure (Landau levels) and the THC  $\sigma_{xy}$  for the square lattice in a uniform magnetic field. Blue lines show the same for the Néel skyrmion crystal in the presence of Rashba SOC, with strength  $\alpha_R^0$  so that the magnetic field is maximally uniform as discussed in the text.

We know the SOC can modify the emergent magnetic field produced by the skyrmion spin texture. For the case of Néel skyrmion with Rashba SOC, we obtain one optimal value  $\alpha_R^0$  where the non-uniformity in the magnetic field distribution is minimized. At  $\alpha_R^0$ , the average of subbands energies is compared to the energies of the Landau levels formed due to hopping of electrons in the square lattice in the presence of a uniform magnetic field, which is shown in Fig. 11(a). Not only the subband energies but also the subband dispersions are comparable to that of Landau levels in a square lattice under a uniform magnetic field, as shown in the figure. As a result, the quantization plateaus of THC become more prominent, similar to those observed in a square lattice subjected to a uniform magnetic field.

### C. Calculation of emergent magnetic field from phase factor

The SOC term introduces two changes in the electron motion: One, it modifies the emergent magnetic field due to the skyrmion and Two, it changes the magnitude of the effective hopping between the lattice sites in the crystal. We illustrate both effects below for the Rashba SOC case.

To calculate the emergent magnetic field, we take a square loop of side  $a$  positioned at the point  $(x, y)$  (see Figure 12), compute the Peierls phase as we traverse around the loop, which gives us the flux through the square, and we then take the limit  $a \rightarrow 0$  to get the magnetic field.

The Rashba SOC Hamiltonian, Eq. (3) of the main

text, has the form  $\mathcal{H}_R = \sum_{\langle ij \rangle} (h_{ij} d_i^\dagger d_j + h_{ij}^* d_j^\dagger d_i)$ , where the effective hopping from site  $j$  to site  $i$  is written in terms of the orientation of the skyrmion spins  $(\theta_i, \phi_i)$  as

$$\begin{aligned}
 h_{ij} &= \left( -t \cos \frac{\theta_i}{2} \cos \frac{\theta_j}{2} - t \cos(\phi_j - \phi_i) \sin \frac{\theta_i}{2} \sin \frac{\theta_j}{2} \right. \\
 &+ \left. \alpha_R (r_y \sin \phi_j + r_x \cos \phi_j) \cos \frac{\theta_i}{2} \sin \frac{\theta_j}{2} - \alpha_R (r_y \sin \phi_i + r_x \cos \phi_i) \sin \frac{\theta_i}{2} \cos \frac{\theta_j}{2} \right) \\
 &+ i \left( -t \sin(\phi_j - \phi_i) \sin \frac{\theta_i}{2} \sin \frac{\theta_j}{2} - \alpha_R (r_y \cos \phi_j - r_x \sin \phi_j) \cos \frac{\theta_i}{2} \sin \frac{\theta_j}{2} \right. \\
 &\left. - \alpha_R (r_y \cos \phi_i - r_x \sin \phi_i) \sin \frac{\theta_i}{2} \cos \frac{\theta_j}{2} \right) \\
 &= t'_{ij} e^{i\delta_{ij}}
 \end{aligned} \tag{29}$$

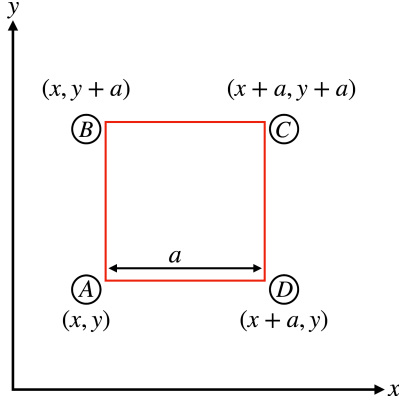


FIG. 12. A schematic diagram of a square loop explaining the four complex hoppings that are used to compute the magnetic field in the text. The four vertices and their cartesian coordinates are shown.

where,  $\delta_{ij} = \tan^{-1}(\text{Im}(h_{ij})/\text{Re}(h_{ij}))$ , and in this equation we have defined  $\mathbf{r} \equiv \mathbf{r}_{ij}$  for simplicity. As described in the main text, the magnetic field due to complex hopping of electron can be computed by adding the phase factors of the hopping terms around a closed loop. Here, we take a small square loop (see Figure 12) and add the four phase factors to get the magnetic flux associated with that loop and from there we obtain the magnetic

field. Below we provide a detail derivation of the magnetic field.

1. First, we consider an infinitesimal square of side ‘ $a$ ’ (i.e.,  $a \rightarrow 0$ ) connecting four lattice sites of the skyrmion as shown in Figure 12. The  $(\theta, \phi)$  profile of the skyrmion spins at these four sites is given by,

$$\begin{aligned}
 \theta_A &= \pi \left( 1 - \frac{r}{\lambda} \right), \\
 \phi_A &= m \tan^{-1} \left( \frac{y}{x} \right) + \gamma,
 \end{aligned} \tag{30}$$

$$\begin{aligned}
 \theta_B &= \pi \left( 1 - \frac{r}{\lambda} - \frac{ay}{r\lambda} \right), \\
 \phi_B &= m \tan^{-1} \left( \frac{y+a}{x} \right) + \gamma,
 \end{aligned} \tag{31}$$

$$\begin{aligned}
 \theta_C &= \pi \left( 1 - \frac{r}{\lambda} - \frac{a(x+y)}{r\lambda} \right), \\
 \phi_C &= m \tan^{-1} \left( \frac{y+a}{x+a} \right) + \gamma,
 \end{aligned} \tag{32}$$

$$\begin{aligned}
 \theta_D &= \pi \left( 1 - \frac{r}{\lambda} - \frac{ax}{r\lambda} \right), \\
 \phi_D &= m \tan^{-1} \left( \frac{y}{x+a} \right) + \gamma
 \end{aligned} \tag{33}$$

2. Next, we calculate the phase factors of the complex hoppings between two consecutive sites along the closed path  $A - B - C - D - A$ . These four phase factors for a single-turned skyrmion can be written as,

$$\begin{aligned} \delta_{AB} = & \tan^{-1} \left[ \left( \frac{ax}{2r^2} \right) \left( 1 - \cos \frac{\theta_A + \theta_B}{2} \right) + \left( \frac{\alpha_R a}{t} \right) \left( \left( \frac{x}{r} \sin \frac{\theta_A + \theta_B}{2} - \frac{axy}{r^3} \cos \frac{\theta_A}{2} \sin \frac{\theta_B}{2} \right) \cos \gamma \right. \\ & \left. - \left( \frac{y}{r} \sin \frac{\theta_A + \theta_B}{2} + \left( \frac{a}{r} - \frac{ay^2}{r^3} \right) \cos \frac{\theta_A}{2} \sin \frac{\theta_B}{2} \right) \sin \gamma \right] \end{aligned} \quad (34)$$

$$\begin{aligned} \delta_{BC} = & \tan^{-1} \left[ \left( -\frac{ay}{2r^2} \right) \left( 1 - \cos \frac{\theta_B + \theta_C}{2} \right) + \left( \frac{\alpha_R a}{t} \right) \left( -\left( \frac{1}{r} (y + a - \frac{ay^2}{r^2}) \sin \frac{\theta_B + \theta_C}{2} - \frac{axy}{r^3} \cos \frac{\theta_B}{2} \sin \frac{\theta_C}{2} \right) \cos \gamma \right. \\ & \left. - \left( \left( \frac{x}{r} - \frac{axy}{r^2} \right) \sin \frac{\theta_B + \theta_C}{2} + \left( \frac{a}{r} - \frac{ax^2}{r^3} \right) \cos \frac{\theta_B}{2} \sin \frac{\theta_C}{2} \right) \sin \gamma \right] \end{aligned} \quad (35)$$

$$\begin{aligned} \delta_{CD} = & \tan^{-1} \left[ \left( -\frac{ax}{2r^2} \right) \left( 1 - \cos \frac{\theta_C + \theta_D}{2} \right) + \left( \frac{\alpha_R a}{t} \right) \left( -\left( \frac{1}{r} (x + a - \frac{ax^2}{r^2}) \sin \frac{\theta_C + \theta_D}{2} - \frac{axy}{r^3} \sin \frac{\theta_C}{2} \cos \frac{\theta_D}{2} \right) \cos \gamma \right. \\ & \left. + \left( \left( \frac{y}{r} - \frac{axy}{r^3} \right) \sin \frac{\theta_C + \theta_D}{2} + \left( \frac{a}{r} - \frac{ay^2}{r^3} \right) \sin \frac{\theta_C}{2} \cos \frac{\theta_D}{2} \right) \sin \gamma \right] \end{aligned} \quad (36)$$

$$\begin{aligned} \delta_{DA} = & \tan^{-1} \left[ \left( \frac{ay}{2r^2} \right) \left( 1 - \cos \frac{\theta_D + \theta_A}{2} \right) + \left( \frac{\alpha_R a}{t} \right) \left( \left( \frac{y}{r} \sin \frac{\theta_D + \theta_A}{2} - \frac{axy}{r^3} \sin \frac{\theta_D}{2} \cos \frac{\theta_A}{2} \right) \cos \gamma \right. \\ & \left. + \left( \frac{x}{r} \sin \frac{\theta_D + \theta_A}{2} + \left( \frac{a}{r} - \frac{ax^2}{r^3} \right) \sin \frac{\theta_D}{2} \cos \frac{\theta_A}{2} \right) \sin \gamma \right] \end{aligned} \quad (37)$$

3. Finally, by adding these phase factors and neglecting 3rd and higher order terms of  $a^2$ , the total magnetic flux can be obtained in the following form.

$$\begin{aligned} B_{SK}^R(r) &= \lim_{a \rightarrow 0} \frac{1}{a^2} \left( \frac{\hbar}{e} \right) (\delta_{AB} + \delta_{BC} + \delta_{CD} + \delta_{DA}) \\ &= \frac{\Phi_0}{2\pi} \times \left[ \frac{\pi}{2\lambda r} \sin \frac{\pi r}{\lambda} \right. \\ &\quad \left. - \frac{\alpha_R}{t} \left( \frac{\pi}{\lambda} \cos \frac{\pi r}{\lambda} + \frac{1}{r} \sin \frac{\pi r}{\lambda} \right) \cos \gamma \right] \end{aligned} \quad (38)$$

From the above equation, we can see that the contribution of SOC in magnetic field distribution is zero if  $\cos \gamma = 0$ . Therefore, the band topology remains unchanged with SOC in this case. But it still contributes to the hopping of electrons between two sites. As a result, it contributes to the THC when the partial filling of the subbands is considered. Here, we provide an example of Bloch skyrmion with  $\gamma = \pi/2$ .

4. As an example, we consider a square loop with the coordinates of four vertices  $A$ ,  $B$ ,  $C$  and  $D$  as  $(x, 0)$ ,  $(x, a)$ ,  $(x + a, a)$ , and  $(x + a, 0)$ , respectively, where  $x \gg a$ . From Eq. (29), the magnitude of four hoppings around this square loop can be written as,

$$|t'_{AB}|^2 = t^2 + \left( -t \frac{a}{x} \cos^2 \frac{\pi x}{2\lambda} + \alpha_R \frac{a^2}{2x} \sin \frac{\pi x}{\lambda} \right)^2 \quad (39)$$

$$\begin{aligned} |t'_{BC}|^2 &= \left( -t \cos \frac{\pi a}{2\lambda} + \alpha_R \frac{a^2}{x} \sin \frac{\pi a}{2\lambda} \right)^2 \\ &+ \left( -t \left( \frac{a}{x+a} - \frac{a}{x} \right) \cos^2 \frac{\pi x}{2\lambda} + \alpha_R a \sin \frac{\pi x}{\lambda} \right)^2 \end{aligned} \quad (40)$$

$$\begin{aligned} |t'_{CD}|^2 &= t^2 + \left( t \frac{a}{x+a} \cos^2 \frac{\pi(x+a)}{2\lambda} \right. \\ &\quad \left. - \alpha_R \frac{a}{2} \frac{a}{x+a} \sin \frac{\pi(x+a)}{\lambda} \right)^2 \end{aligned} \quad (41)$$

$$|t'_{DA}|^2 = \left( t \cos \frac{\pi a}{2\lambda} \right)^2 + \left( \alpha_R a \sin \frac{\pi x}{\lambda} \right)^2 \quad (42)$$

From the above set of equations, if the phases of all hoppings are added, the coefficients of  $\alpha_R$  cancel each other, but its contribution is present in the individual hopping magnitudes. Hence, although the band topology and THC remain unaffected by Rashba SOC for the case of Bloch skyrmion with  $\gamma = \pi/2$ , the individual effective hopping and the THC of partially filled bands are modified by Rashba SOC.

In a similar process, the magnetic field for all other cases can be computed, which are given in Eq. (6) and (14)-(17) in the main text.

#### D. Equivalence of electronic Hamiltonian with Rashba, Dresselhaus, and Weyl SOC

As explained in the main text, the Hamiltonian (and therefore the magnetic field as well) with Dresselhaus and Weyl SOC can be mapped to the Hamiltonian with Rashba SOC. Here, we provide explicit examples for two cases.

Case I. Néel skyrmion with helicity  $\gamma = 0$  and Rashba SOC vs. Bloch skyrmion with helicity  $\gamma = \pi/2$  and Weyl SOC.

Using Eqs. (3) and (13) of the main text, the hopping terms between two sites are written as



$$\begin{aligned}
h_R^{ij} = & (-t) \cos \frac{\theta_{ij}}{2} e^{ia_{ij}} - i\alpha_R [(r_{ij}^y \cos \alpha_j - r_{ij}^x \sin \alpha_j) + i(r_{ij}^x \cos \alpha_j + r_{ij}^y \sin \alpha_j)] \cos \frac{\theta_i}{2} \sin \frac{\theta_j}{2} \\
& + ((r_{ij}^y \cos \alpha_i - r_{ij}^x \sin \alpha_i) - i(r_{ij}^x \cos \alpha_i + r_{ij}^y \sin \alpha_i) \cos \frac{\theta_j}{2} \sin \frac{\theta_i}{2}), \tag{43}
\end{aligned}$$

$$\begin{aligned}
h_W^{ij} = & (-t) \cos \frac{\theta_{ij}}{2} e^{ia_{ij}} - i\alpha_W [(r_{ij}^y \cos \alpha_j - r_{ij}^x \sin \alpha_j) + i(r_{ij}^x \cos \alpha_j + r_{ij}^y \sin \alpha_j)] \cos \frac{\theta_i}{2} \sin \frac{\theta_j}{2} \\
& + ((r_{ij}^y \cos \alpha_i - r_{ij}^x \sin \alpha_i) - i(r_{ij}^x \cos \alpha_i + r_{ij}^y \sin \alpha_i) \cos \frac{\theta_j}{2} \sin \frac{\theta_i}{2}). \tag{44}
\end{aligned}$$

These two Hamiltonians are identical term by term:  $h_R^{ij} = h_W^{ij}$  for the same SOC strength  $\alpha_R = \alpha_W$ . This means that all electronic properties are the same for the two cases including the emerging magnetic field and the THC.

---

Case II. Néel skyrmion with helicity  $\gamma = 0$  and Rashba SOC vs. Bloch antiskyrmion with helicity  $\gamma = \pi/2$  and Dresselhaus SOC.

The hopping term between two sites for the first scenario is already given in Eq. (43). The hopping term for the second scenario from Eq. (12) of the main text is

$$\begin{aligned}
h_D^{ij} = & (-t) \cos \frac{\theta_{ij}}{2} e^{-ia_{ij}} - i\alpha_D [(-r_{ij}^y \cos \alpha_j + r_{ij}^x \sin \alpha_j) + i(r_{ij}^x \cos \alpha_j + r_{ij}^y \sin \alpha_j)] \cos \frac{\theta_i}{2} \sin \frac{\theta_j}{2} \\
& + ((-r_{ij}^y \cos \alpha_i + r_{ij}^x \sin \alpha_i) - i(r_{ij}^x \cos \alpha_i + r_{ij}^y \sin \alpha_i) \cos \frac{\theta_j}{2} \sin \frac{\theta_i}{2}). \tag{45}
\end{aligned}$$

From Eq. (43) and (45), one can easily see that  $h_R^{ij} = h_D^{ij*}$ , which are complex conjugates of each other. So, the electronic properties are related to each other via a sym-

---

metry transformation. For instance, the emergent magnetic field is same in magnitude but opposite in direction, which makes the THC also the same in magnitude but opposite in sign.